Mode Characteristics of Radio-Frequency Atmospheric Glow Discharges

Jianjun Shi and Michael G. Kong, *Senior Member, IEEE*

***Abstract*—Building on recent experimental and numerical evidence of different glow modes in atmospheric plasmas, this paper reports a systematic study of these modes in radio-frequency (RF) glow discharges in atmospheric helium. Using a one-dimensional (1-D) hybrid computer model, we present detailed characterization of three glow modes, namely the α mode, the $\alpha-\gamma$ transitional mode, and the γ-mode in a 13.56-MHz atmospheric glow discharge over a wide range of root mean square (RMS) current density from 5 $\mathrm{mA/cm^2}$ to 110 $\mathrm{mA/cm^2}$. Our focus is on sheath dynamics through spatial and temporal profiles of charged densities, electric field, electron mean energy, sheath thickness, and sheath voltage, and when appropriate our results are compared against experimental data of atmospheric glow discharges and that of glow discharges at reduced gas pressure below 1 torr. Fundamental characteristics of the three glow modes are shown to be distinctively different, and these can be used as a hitherto unavailable route to tailor the operation of radio-frequency atmospheric glow discharges to their intended applications.**

***Index Terms*—Atmospheric glow discharges, glow modes, helium, mode transition, numerical simulation, radio frequency.**

I. Introduction

ATMOSPHERIC pressure glow discharges (APGD) generated at radio frequencies (RF) at megahertz are used increasingly for many technologically important applications including etching, deposition, surface modification, and decontamination [1]–[9]. They are capacitively coupled plasmas generated usually between two bare metallic electrodes and typically at 13.56 MHz. Their operation is also very versatile, helped partly by their low-breakdown voltage. Through largely an engineering development, their application range and capability have been expanded considerably [1], [6], [9]. Yet there is a fundamental need for substantially advancing their basic understanding in order to aid not only the interpretation of complex experimental observations but also the development of their diagnostics methodologies. One missing element in the current understanding is whether there are different operation regimes, or glow modes, in RF APGD similar to low-pressure glow discharges. If this is the case, it will be possible to tailor operation characteristics of RF APGD to the specific requirements of their intended applications.

Recent experimental and numerical studies suggest that there are indeed different glow modes, including both the α mode and the γ mode, in radio-frequency atmospheric discharges [8], [10]. These preliminary studies have established that the α mode operates at low-current densities, whereas the γ mode operates at high current densities. Secondary electron emissions have been shown to be important in the γ mode but not in the α mode. Furthermore, it has been demonstrated that the α mode has better discharge stability, whereas the γ mode produces more abundant plasma species including charged particles and metastables [10]. However, what remains unknown is how signatures of different modes of RF APGD are reflected in their operation parameters that can be readily measured, for example, the current–voltage characteristics. If such electrical signatures can be captured, it will be possible to lock RF APGD operation in a preferred glow mode such that the desired plasma properties, either good plasma stability or abundant plasma species, can be maintained electrically. For continuous material processing using RF APGD, particularly on an industrial scale, this would be an important capability of profound implications. To this end, it is essential to establish a thorough understanding of the operational characteristics of the α and γ modes.

In this paper, we focus on sheath dynamics by means of spatial and temporal profiles of electric field, sheath thickness, sheath voltage, electron mean energy, and electron density. Many of these physical quantities are currently very difficult to measure, because RF APGD are generated typically in a sub-cm gas gap usually with their sheath thickness below 300 μm and their electron density less than 10^{13} $\mathrm{cm^{-3}}$ [8]. As a result, we take a computational approach using a self-consistent fluid model. This paper is organized as follows. After an introduction to the numerical model in Section II, we will present simulation data of the current–voltage characteristics in Section III. Then in Section IV, sheath dynamics will be discussed with the aid of spatial and temporal profiles of sheath thickness, sheath voltage, electron energy, electric field, and electron density. Finally, in Section V, the findings reached in the previous sections will be summarized.

II. Computational Model

Our study is based on a one-dimensional (1-D) self-consistent hybrid model developed for atmospheric pressure glow discharges, in which electrons are described kinetically and all other plasma species are described hydrodynamically [10], [11]. This model has been experimentally validated [10], [11], and is similar to fluid models developed for low-pressure glow discharges [12] and for atmospheric pressure glow discharges [13]. Discharge characteristics are computationally studied in the direction perpendicular to the electrode plane by solving the governing equations for each species in the plasma, Poisson equation for the electric field across the discharge gap, and the electron energy conservation equation for the electron temperature.

Manuscript received September 9, 2004; revised November 12, 2004.

The authors are with the Department of Electronic and Electrical Engineering, Loughborough University, Leicestershire LE11 3TU, U.K. (e-mail: m.g.kong@lboro.ac.uk).

Digital Object Identifier 10.1109/TPS.2005.844527

The 1-D continuity equations for different plasma species are given as

$$\frac{\partial n_k}{\partial t} + \frac{\partial \Gamma_k}{\partial x} = S_k \tag{1}$$

where $n_{\boldsymbol{k}}$ and $\Gamma_{\boldsymbol{k}}$ are, respectively, the number density and the flux density of one plasma species ($\boldsymbol{k}$). S_k is the source term of the $\boldsymbol{k}$ species, representing the net contribution of production and destruction rates of the $\boldsymbol{k}$ species via each of relevant elementary reactions. Plasma species considered in this simulation include the electron e, the helium ion He^+, the dimer helium ion He_2^+, the excited helium atoms He^* (including both $\mathrm{He}(2^1\mathrm{S})$ and $\mathrm{He}(2^3\mathrm{S})$ metastables), and the excited dimer helium He_2^*. Although impurities are important in practical helium RF APGD, this study is concerned with generic features of their glow modes and as such the effects of impurities are ignored as justified in our early study [10].

The flux density for each species is evaluated by the drift-diffusion approximation

$$\Gamma_k = -D_k \frac{\partial n_k}{\partial x} \pm \mu_k n_k E \tag{2}$$

where diffusion coefficient D_k and mobility μ_k for each species are obtained from the literature [13]. The second term on the right-hand side of (2) is positive for positive ions and negative for electrons. The electric field in the discharge gap is calculated from Poisson equation

$$\varepsilon_0 \frac{\partial E}{\partial x} = -e\left(\sum_p n_p - n_e\right) \tag{3}$$

where n_p and n_e are, respectively, densities of positive ions and electrons, and ε_0 is the vacuum permittivity. To determine the boundary condition for Poisson equation, the current continuity equation is applied to the entire discharge gap and is given below as follows:

$$J(t) = J_0 \sin(2\pi f t) = \varepsilon_0 \frac{\partial E}{\partial t} - \left(-e\Gamma_e + e\sum_p \Gamma_{+,p}\right) \tag{4}$$

where J_0 is the magnitude of the current density and f is the excitation frequency. For RF APGD, (4) is applied to the midpoint of the discharge gap where the contribution of space charges to the electric field is at its lowest [10], [13].

Instead of using the local electric field to evaluate elementary reaction rates, the electron mean energy is used. This is important in order to accurately describe plasma dynamics in the electrode sheath region [11] where hydrodynamic models are inadequate [14], [15]. The energy conservation equation for electrons considers thermal heating of electrons by the electric field as well as the energy loss/gain from their inelastic and elastic collisions with different plasma species. More specifically it is given as follows:

$$\frac{\partial(n_e\varepsilon)}{\partial t} = -\frac{\partial \Gamma_\varepsilon}{\partial x} - e\Gamma_e E - K_{L,ie}(\varepsilon) n_i n_e - 3\frac{m_e}{m_{\mathrm{neut}}} N K_{mt} n_e k (T_e - T_{\mathrm{neut}}) \tag{5}$$

where ε is the electron mean energy and Γ_ε is the flux density of electron energy given by

$$\Gamma_\varepsilon = \frac{5}{3}\Gamma_e \varepsilon - n_e D_e \frac{\partial \varepsilon}{\partial x}. \tag{6}$$

$K_{L,ie}$ is the electron energy loss rate via a reaction between species i and electrons. K_{mt} is the momentum transfer frequency of the elastic collision between electrons and background gas atoms. Their values are taken from [13]. Also, m_e and T_e are electron mass and electron temperature, whereas m_{neut} and T_{neut} are, respectively, mass and temperature of neutral background helium atoms. $T_{\mathrm{neut}} = 300$ K is used throughout our simulation. N is the number density of background helium atoms and k is the Boltzmann constant.

Secondary electron emission due to ion bombardment is also considered in order to evaluate the electron density at the gas-electrode boundary [10]. Similar to the treatment in low-pressure glow discharges [12], the energy of emitted electron is fixed to 0.5 eV. For ions and metastables, it is assumed that their fluxes on the electrodes are dominated by drift fluxes, driven by the electric field, and that their diffusive fluxes are negligible.

III. Current–Voltage Characteristics

As a starting point to the work reported here, we summarize key findings of the previous work on modes in RF atmospheric glow discharges [8], [10]. Experimental data of the current–voltage relationship show distinctively different operation regimes, or glow modes, in a helium RF APGD [8]. At low-current densities, the discharge current increases in proportion to the RF voltage across the electrode gap and the differential conductivity of the plasma is positive. This is similar to the α mode in low-pressure glow discharges, and corresponds to the operation regime of most reported RF APGD experiments [1]–[7], [9], [16]. When the current density increases to a critical threshold, the discharge plasma evolves into a different operation regime in which the discharge current increases with decreasing gap voltage and the differential conductivity becomes negative [8]. This is similar to the γ mode in low-pressure glow discharges. Indeed, a companion numerical study confirms that the low-current regime resembles closely the α mode, whereas the high-current regime corresponds to the γ mode [10]. Ionization in the α mode is volumetric, driven mainly by the oscillatory field of the applied voltage. In contrast, gas ionization in the γ mode is localized near the boundary between the sheath and the quasi-neutral plasma regions and it is largely driven by significant electron acceleration by the sheath electric field [10]. Findings of this previous numerical work are highlighted in Fig. 1 where the electron density is shown as a function of the applied voltage at two different secondary electron emission coefficients. It shows clearly that secondary emission electrons are important when the electron density is large (well above 5×10^{11} cm^{-3}), but not when the electron density is small (well below 1×10^{11} cm^{-3}). The focus of this early numerical study was on mechanisms of these glow modes, and, as such, it did not attempt to study directly many experimentally important features such as the current–voltage characteristics.

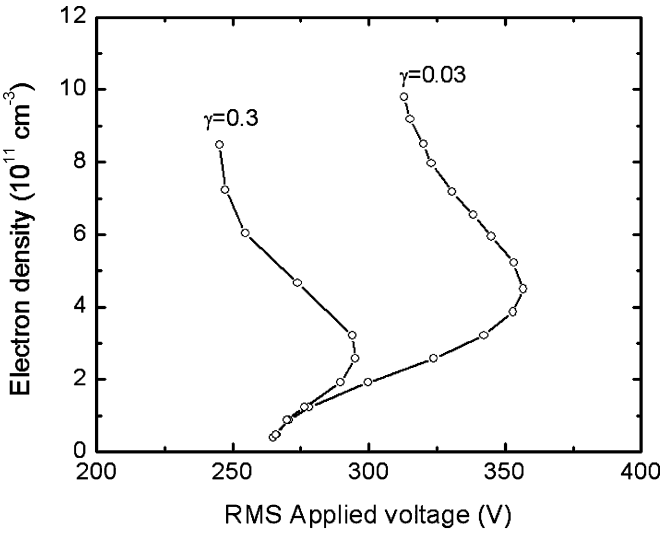

Fig. 1. Electron density as a function of the applied voltage at two different secondary electron emission coefficients in a 13.56 MHz APGD.

Here we consider a 13.56-MHz APGD generated in a pure helium gap at a nominal atmospheric pressure of 760 torr and between two metallic electrodes. The electrode gap distance is 0.4 cm, and the secondary electron emission coefficient is assumed to be at 0.03. Its current–voltage characteristics are shown in Fig. 2(a), in which three operation regimes are clearly seen. These are the α mode in the region-I, the $\alpha - \gamma$ transitional mode in the region-II and the γ mode in the region-III. For all data shown, the waveform of the discharge current remains largely sinusoidal with its harmonic content well below 1%, and, as such, we use its root mean square (RMS) value as a measure of its strength. In the α mode, the gap voltage increases monotonically with the discharge current density and the differential conductivity of the discharge is positive. This trend is identical to that of available RF APGD experiment data [1]–[9], [16] and also consistent with the α mode in low-pressure glow discharges [17], [18]. As the current density increases above 28 $\mathrm{mA/cm^2}$, the gap voltage increases less for a given increment in the discharge current. After the current density goes above 50 $\mathrm{mA/cm^2}$, the gap voltage decreases with increasing current density and the differential conductivity becomes negative. This dependency is generic and is consistent with experimental observation of the γ mode in RF APGD [8]. The gradual transition from the α mode to the γ mode is, however, different from glow discharges at 0.05–0.5 torr for which the $\alpha - \gamma$ transition is abrupt [17]. It is interesting to note that the general trend of the current–voltage relationship is also reflected in the voltage dependence of the electron density, as shown in Fig. 2(b). Here, the electron density is calculated at the gap centre and at the time when the discharge current reaches its peak. Again, in the α mode, the electron density increases monotonically with the gap voltage and continues so into the $\alpha - \gamma$ transitional mode. Once in the γ mode, on the other hand, the electron density increases with decreasing gap voltage. So, there is a clear correlation between the electron density and the discharge current. Significantly, the evolution of the differential conductivity can be monitored easily from current and voltage measurements, and

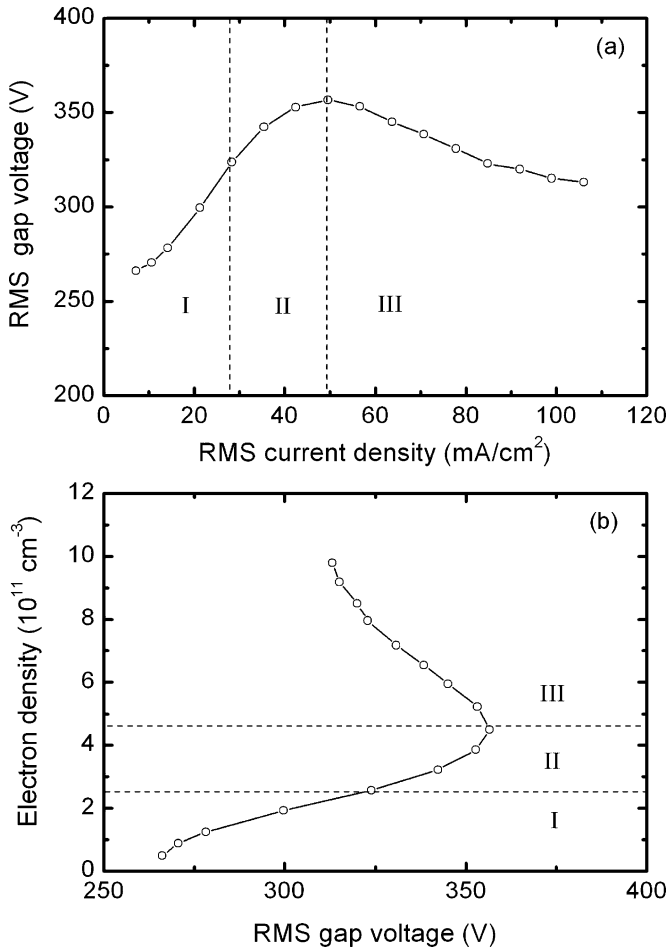

Fig. 2. (a) Current–voltage relationship showing three glow modes, namely the α mode in Region I, the $\alpha - \gamma$ transitional mode in Region II, and the γ mode in Region III. (b) These three glow modes are also evident in the voltage dependence of the electron density.

so can be used to control RF APGD operation either in the α mode or the γ mode.

To provide insight into the mechanisms responsible for different glow modes, we first consider time-averaged spatial profiles of the electron density. In Fig. 3(a), spatial profiles of the time-averaged electron density are shown for three different current density values of 7, 14, and 28 $\mathrm{mA/cm^2}$. The common feature of these three spatial profiles is that they are all bell-shaped with the maximum electron density at the center of the electrode gap. As indicated in Fig. 2, all three cases in Fig. 3(a) are in the α mode where the electron acceleration by the sheath electric field is moderate and most electrons need to penetrate into the quasi-neutral plasma region to acquire sufficiently high-kinetic energy for gas ionization. Consequently, many gas ionization events occur outside the sheath region and most electrons are produced in the quasi-neutral plasma region within which they are trapped by the rapidly oscillatory field of the applied voltage. As the discharge current increases, the sheath electric field increases significantly and its resulting acceleration of electrons becomes sufficient for electrons to ionize helium atoms within the sheath region. When this occurs, considerable gas ionization is induced in the sheath region and electrons thus produced become dominant leading to a density maximum within the sheath

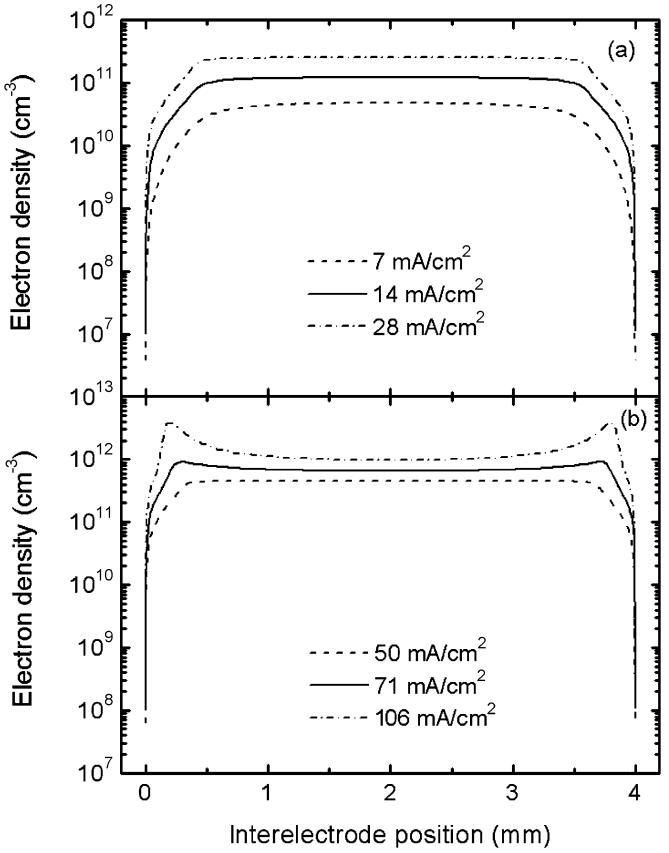

Fig. 3. Spatial profiles of electron density cross the electrode gap are shown in (a) the α mode with an RMS discharge current density at 7, 14, and 28 $\mathrm{mA/cm^2}$ and (b) the γ mode with the discharge current density amplitude of 50, 71, and 106 $\mathrm{mA/cm^2}$.

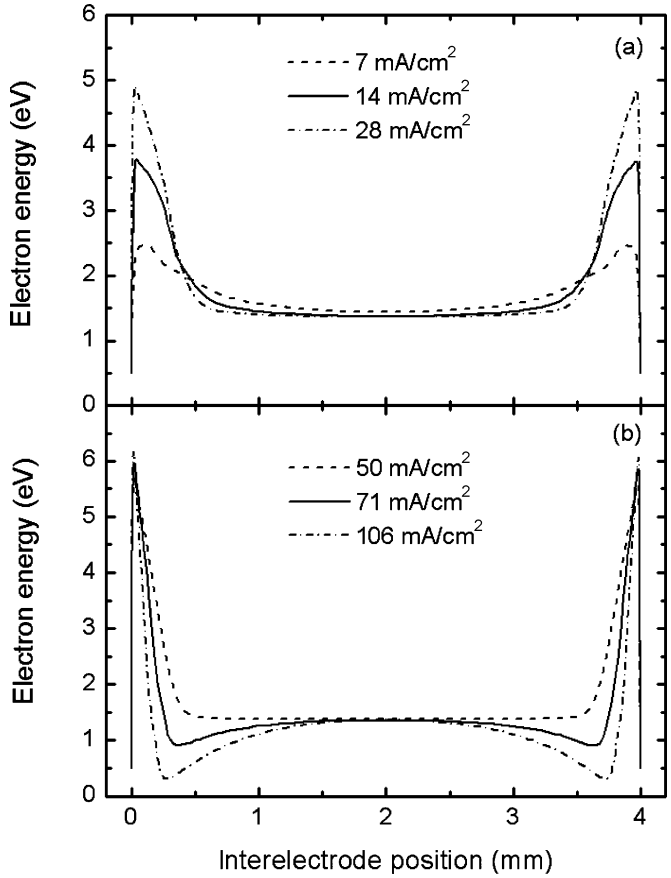

Fig. 4. Spatial profiles of electron mean energy in the electrode gap are shown in (a) the α mode and (b) the γ mode. Conditions are the same as in Fig. 3.

region. Indeed, this is shown in Fig. 3(b) where three cases are shown for current densities at 50 $\mathrm{mA/cm^2}$, 71 $\mathrm{mA/cm^2}$, and 106 $\mathrm{mA/cm^2}$, all in the γ mode.

The current–voltage relationship of Fig. 2 for the α and γ modes in RF APGD are very similar to that observed for RF APGD [4], [5], [8], [9], [16], and also for low-pressure glow discharges [17]–[19]. We will revisit the above discussion in the next section where the electric field and the electron energy are profiled for both the α mode and the γ mode.

IV. Sheath Dynamics

In this section, we consider sheath dynamics in terms of the electron mean energy, the electric field, the sheath voltage, and the sheath thickness. In Fig. 4(a), spatial profiles of time-averaged electrons mean energy are shown for three different current density values of 7, 14, and 28 $\mathrm{mA/cm^2}$ in the α mode. The maximum electron energy occurs near the electrode surface, and its value increases with increasing discharge current from 2.46 eV at 7 $\mathrm{mA/cm^2}$ to 4.91 eV at 28 $\mathrm{mA/cm^2}$. The reduction in the electron energy from its peak is a result of kinetic energy released by electrons via their ionization of helium atoms, and the space between an electrode and the location of the minimum electron energy is where the majority of the gas ionization events take place. With a symmetric spatial profile, the electron energy has its minimum at the center of the electrode gap and its value changes little with increasing discharge current. This suggests that gas ionization events occur over the entire electrode gap in the α mode, and that many electrons need to penetrate into the quasi-neutral plasma region before gaining adequate kinetic energy for gas ionization and subsequently reducing their kinetic energy to its minimum.

When the discharge evolves into its γ mode, Fig. 4(b) suggests that the increase in the peak electron energy is now much smaller than that in the α mode for a given increment in the current density. More specifically, as the current density increases from 50 $\mathrm{mA/cm^2}$ to 106 $\mathrm{mA/cm^2}$, the electron energy increases only 0.4 eV from 5.7 eV to 6.1 eV. Nevertheless, the comparably large electron energies in the γ mode suggest that many electrons are substantially accelerated in the electrode sheath and so capable of inducing gas ionization within the sheath region. This is further supported by the observation in Fig. 4(b) that the minimum electron energy is at the boundary between the sheath region and the quasi-neutral plasma region suggesting that most gas ionization events occur within the sheath region. This supports our discussion of Fig. 3.

Fig. 5(a) shows spatial profiles of the time-averaged electric field in the α mode. The dimension of the sheath region is seen to change little with increasing current density. The maximum electric field is at the electrode surface, and its value changes from 0.88 kV/cm at 7 $\mathrm{mA/cm^2}$ to 4.99 kV/cm at 28 $\mathrm{mA/cm^2}$. Fig. 5(b) presents three additional cases now in the γ mode, where the maximum electric field is seen to change from 8.07 kV/cm at 50 $\mathrm{mA/cm^2}$ to 12.39 kV/cm at 106 $\mathrm{mA/cm^2}$. The

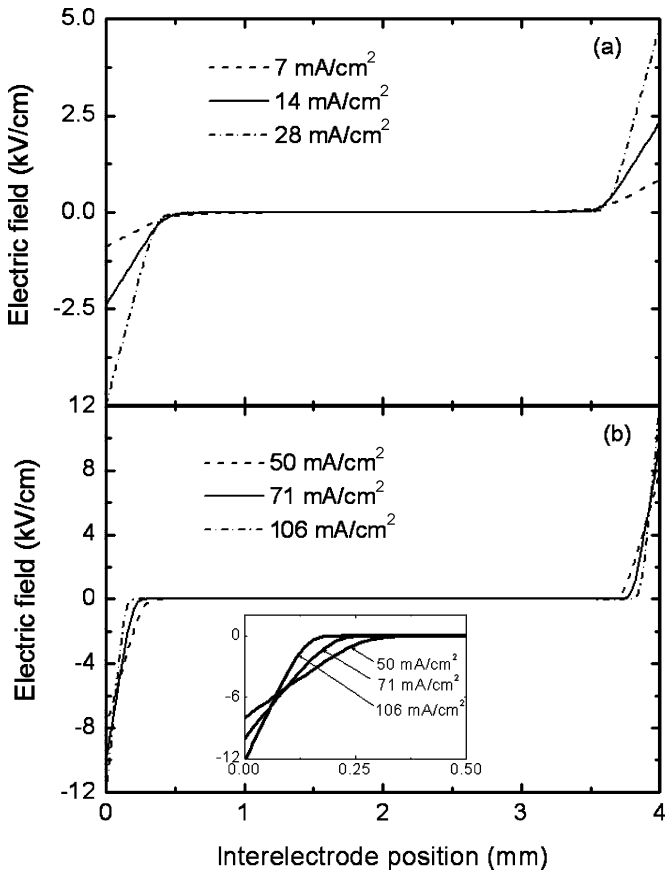

Fig. 5. Spatial profiles of electric field in the electrode gap are shown for (a) the α mode and (b) the γ mode with the same conditions as that in Fig. 3.

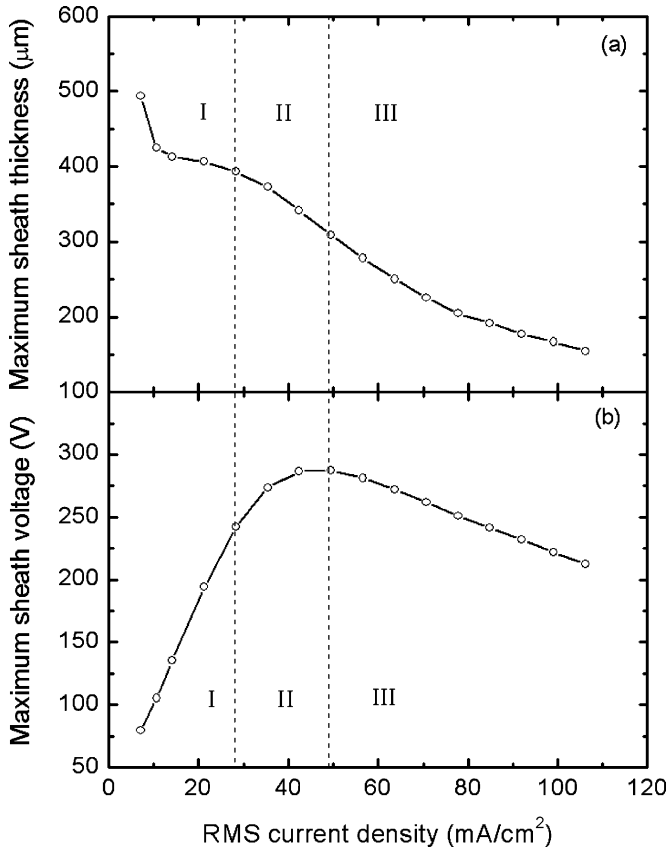

Fig. 6. Sheath characteristics in terms of (a) the maximum sheath thickness and (b) the maximum sheath voltage as a function of the discharge current density, both measured at the time of the peak discharge current. Definition of three regions is identical to that in Fig. 2.

sheath region is characterized by a region of almost linear fall of the electric field, and the sheath thickness shrinks with increasing current density. Against this is similar to sheath dynamics in low-pressure glow discharges [17] and to dc APGD [11], [20]. It is worth mentioning that the electric field reduces from its peak at the electrode surface in an almost linear fashion, particularly in the γ mode, suggesting that it obeys Aston's law [21].

Sheath dynamics can be further understood from the current density dependence of sheath thickness and sheath voltage. In Fig. 6, the peak sheath thickness and the peak sheath voltage calculated at the current maximum are plotted as a function of the current density. The sheath thickness is obtained by evaluating the distance over which the electric field reduces from its peak to 14% of the peak field, a technique used for dc APGD [11]. This technique becomes unpractical at very small current densities because reduction in the electric field within the sheath region is now larger than 14%. So, at low-current densities, we employ an alternative technique by using the distance over which the electric field reduces from its peak value to 1 kV/cm, as used for low-pressure glow discharges [22]. In general, the sheath thickness decreases monotonically as the current density increases. Its value starts above 500 μm in the α mode, and decreases rapidly to about 100 μm at large current densities in the γ mode. These small spatial scales highlight the difficulties for probe-based diagnostic methodologies. On the other hand, the current dependence of the sheath voltage shows clear distinction of different glow modes and its profile maps closely onto the current dependence of the gap voltage of Fig. 2(a). Also interesting is the observation that the sheath voltage takes up most of the gap voltage at large current densities.

The contrasting characteristics of the three glow modes can also be seen in the maximum electron generation rate, $G_{e,\max}$, and in the voltage–current phase angle. $G_{e,\max}$ is electrons produced per second per cm^3 through inelastic collisions. In Fig. 7, it is seen to depend weakly on the current density in the α mode and strongly in the γ mode. In Fig. 8, the voltage–current phase angle is plotted as a function of the discharge current density and again the existence of the three glow modes is clear. In general, the phase angle reduces as the current density increases, suggesting an increment in the electrical conductivity of the discharge plasma and a simultaneous reduction in plasma reactance. The plasma is more capacitive in the α mode, particularly at low-current densities, and as the current density increases it becomes less capacitive and more conductive. It is worth mentioning that the sheath thickness decreases with increasing current density, as shown in Fig. 6(a), and so sheath reactance $1/\omega C_{\rm sh} = d_{\rm sh}/e\omega A$ decreases. Here, $d_{\rm sh}$ is the sheath thickness, A is the cross-sectional area of the plasma, ω is the angular frequency, and $C_{\rm sh}$ is the sheath capacitance. The decreasing trend of the voltage–current phase angle suggests that the reduction in plasma resistance is not as much as the reduction in the sheath reactance. In the γ mode, the phase angle re-

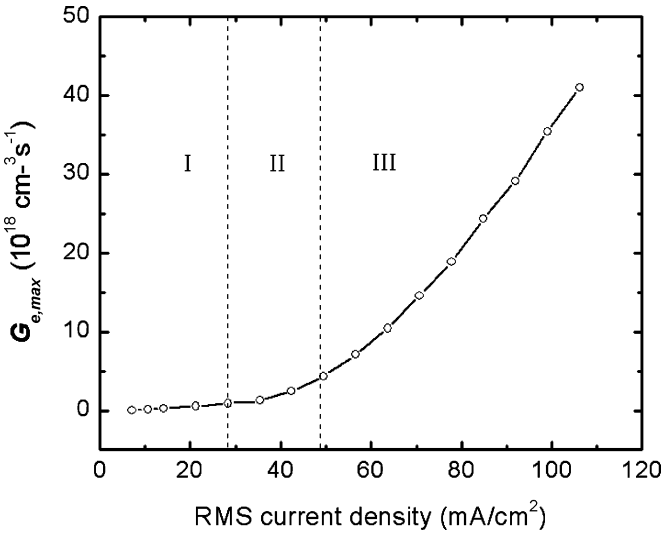

Fig. 7. Maximum electron generation rate in the electrode gap as a function of the current density. Definition of the three regions is identical to that in Fig. 2.

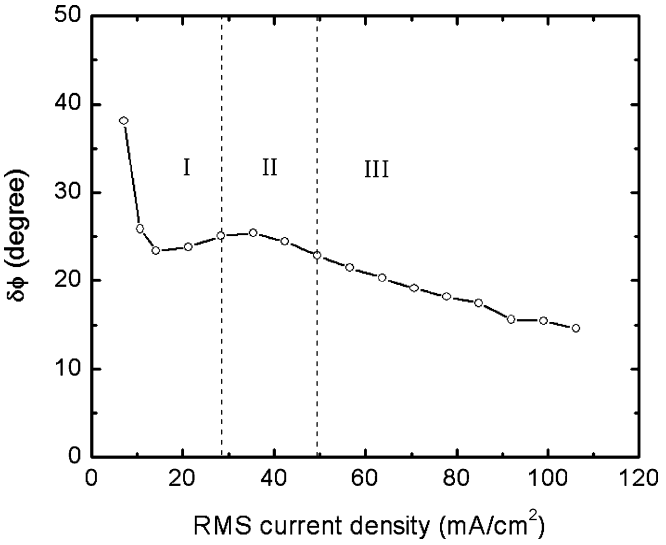

Fig. 8. Dependence of the voltage-current phase difference on the discharge current density with the definition of the three regions identical to that in Fig. 2.

duces more rapidly with increasing current. This is consistent with the more rapid reduction of the sheath thickness in the γ mode of Fig. 6(a). The above findings are in agreement with experimental observations of RF APGD [8] and support the circuit model of the plasma proposed previously [11]. It is also worth mentioning that the relatively constant phase between $20\text{-}\mathrm{mA/cm^2}$ 40 $\mathrm{mA/cm^2}$ may be used experimentally to indicate the boundary between the α mode and the γ mode.

V. Conclusion

In this paper, a detailed characterization study was presented for the three glow modes of RF atmospheric glow discharges, namely the α mode, the $\alpha - \gamma$ transitional mode, and the γ mode. Numerically obtained current–voltage relationship was shown to agree with relevant experimental data for RF APGD and for RF low-pressure glow discharges. More specifically, the α mode has a positive differential conductivity, whereas the γ mode has a negative differential conductivity. This difference in the differential conductivity can be used to achieve simple experimental control of the operation mode of RF APGD. Also, it was demonstrated that the $\alpha - \gamma$ transitional phase has a relatively constant voltage-current phase and this feature can also be used to identify experimentally the operation boundary between the α mode and the γ mode. Further insights were provided into the sheath dynamics of RF APGD in each of their three glow modes. These should be useful for both the design and the interpretation of RF APGD experiments.

References

[1] H. Koinuma, H. Ohkubo, T. Hashimoto, K. Inomata, T. Shiraishi, A. Miyanaga, and S. Hayashi, "Development and application of a microbeam plasma generator," *Appl. Phys. Lett.*, vol. 60, pp. 816–817, Feb. 1992.

[2] J. Y. Jeong, S. E. Babayan, V. J. Tu, J. Park, I. Henins, R. F. Hicks, and G. S. Selwyn, "Etching materials with an atmospheric-pressure plasma jet," *Plasma Sources Sci. Technol.*, vol. 7, pp. 282–285, Aug. 1998.

[3] H. Yoshiki, A. Oki, H. Ogawa, and Y. Horiike, "Generation of a capacitively coupled microplasma and its application to the inner-wall modification of a poly(ethylene terephthalate) capillary," *J. Vac. Sci. Technol. A, Vac. Surf. Films*, vol. 20, pp. 24–29, Jan./Feb. 2002.

[4] E. Stoffels, A. J. Flikweert, W. W. Stofels, and G. M. Kroesen, "Plasma needle: A nondestructive atmospheric plasma source for fine surface treatment of (bio)materials," *Plasma Sources Sci. Technol.*, vol. 11, pp. 383–388, Nov. 2002.

[5] Y.-B. Guo and F. C.-N. Hong, "Radio-frequency microdischarge arrays for large-area cold atmospheric plasma generation," *Appl. Phys. Lett.*, vol. 82, pp. 337–339, Jan. 2003.

[6] L. Baars-Hibbe, P. Sichler, C. Schrader, C. Gessner, K. H. Gericke, and S. Buttgenbach, "Micro-structured electrode arrays: Atmospheric pressure plasma processes and applications," *Surf. Coatings Technol.*, vol. 174, pp. 519–523, Sep./Oct. 2003.

[7] A. P. Yalin, Z. Q. Yu, O. Stan, K. Hoshimiya, A. Rahman, V. K. Surla, and G. J. Collins, "Electrical and optical emission characteristics of radio-frequency-driven hollow slot microplasmas operating in open-air," *Appl. Phys. Lett.*, vol. 83, pp. 2766–2768, Oct. 2003.

[8] J. J. Shi, X. T. Deng, R. Hall, J. D. Punnett, and M. G. Kong, "Three modes in a radio frequency atmospheric pressure glow discharge," *J. Appl. Phys.*, vol. 94, pp. 6303–6310, Nov. 2003.

[9] S. Y. Moon, W. Choe, and B. K. Kang, "A uniform glow discharge plasma source at atmospheric pressure," *Appl. Phys. Lett.*, vol. 84, pp. 188–190, Jan. 2004.

[10] J. J. Shi and M. G. Kong, "Mechanisms of α and γ modes in radio-frequency atmospheric glow discharges," *J. Appl. Phys.*, vol. 97, Jan. 2005.

[11] ——, "Cathode fall characteristics in a DC atmospheric pressure glow discharge," *J. Appl. Phys.*, vol. 94, pp. 5504–5513, Nov. 2003.

[12] E. Gogolides and H. H. Swain, "Continuum modeling of radio-frequency glow discharge. I. Theory and results for electropositive and electronegative gases," *J. Appl. Phys.*, vol. 72, pp. 3971–3987, Nov. 1992.

[13] X. Yuan and L. L. Raja, "Computational study of capacitively coupled high-pressure glow discharges in helium," *IEEE Trans. Plasma Sci.*, vol. 31, no. 4, pp. 495–503, Aug. 2003.

[14] Y. B. Golubovskii, V. A. Maiorov, J. Behnke, and J. F. Behnke, "Modeling of the homogeneous barrier discharge in helium at atmospheric pressure," *J. Phys. D, Appl. Phys.*, vol. 36, pp. 39–49, Feb. 2003.

[15] M. G. Kong and X. T. Deng, "Electrically efficient production in a diffuse nonthermal atmospheric plasma," *IEEE Trans. Plasma Sci.*, vol. 31, no. 1, pp. 7–18, Feb. 2003.

[16] J. Park, I. Henins, H. W. Herrmann, G. S. Selwyn, and R. F. Hicks, "Discharge phenomena of an atmospheric pressure RF capacitive plasma source," *J. Appl. Phys.*, vol. 89, pp. 20–28, Jan. 2001.

[17] V. A. Lisovskii, "Features of the $\alpha - \gamma$ transition in a low-pressure RF argon discharge," *Tech. Phys.*, vol. 43, pp. 526–534, May 1998.

[18] P. Vidaud, S. M. A. Durrani, and D. R. Hall, "Alpha and gamma RF capacitive discharges in $\mathrm{N_2}$ at intermediate pressures," *J. Phys. D, Appl. Phys.*, vol. 21, pp. 57–66, Jan. 1988.

[19] I. V. Schweigert, "Different modes of a capacitively coupled radio-frequency discharge in methane," *Phys. Rev. Lett.*, vol. 92, Apr. 2004.

[20] A. Bogaerts and R. Gijbels, "Similarities and differences between direct current and radio-frequency glow discharges: A mathematical simulation," *J. Ann. At. Spectrom.*, vol. 15, pp. 1191–1201, Sep. 2000.

[21] J. R. Roth, *Industrial Plasma Engineering, Vol. 1—Principles*. Bristol, U.K.: Inst. Phys. Press, 1995, ch. 9.
[22] S. Yonemura, K. Nanbu, and N. Iwata, "Synthesis of sheath voltage drops in asymmetric radio-frequency discharges," *J. Appl. Phys.*, vol. 96, pp. 127–132, Jul. 2004.

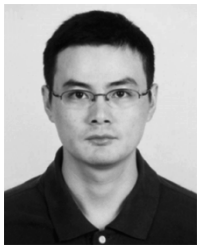

Jianjun Shi received the B.Sc. and M.Sc. degrees in physics from Nanjing University, Nanjing City, China, in 1999 and 2002, respectively, and is currently working toward the Ph.D. degree at Loughborough University, Leicestershire, U.K.

His interests include atmospheric pressure glow discharges and their applications.

Michael G. Kong (M'94–SM'98) received the B.Sc. and M.Sc. degrees, in electronics engineering from Zhejiang University, Zhejiang, China, in 1984 and 1987, respectively, and the Ph.D. degree in electrical engineering from Liverpool University, Liverpool, U.K., in 1992.

After postdoctoral positions at Liverpool University and Nottingham University, Nottingham, U.K., he joined Liverpool University as a Lecturer in 1995. In 1999, he joined Loughborough University, Leicestershire, U.K., where he holds a Chair in Bioelectrical Engineering. At Loughborough University, he is also Head of Power and Renewable Energy Division, whose research encompasses plasmas, pulsed power, and renewable energy. His research interests include atmospheric pressure glow discharges, compact waveguide free electron lasers, and power systems and devices. In these subject areas, he has published some 120 papers in scientific journals and peer-reviewed conference proceedings.